https://doi.org/10.17221/106/2025-SWR

Ca–Mg–Al LDH-modified wheat straw biochar for efficient lead chemisorption from aqueous solution: Insights from isotherm and kinetic analyses

Muhammad Tahir Amin[1], Abdulrahman Ali Alazba[2,3], Muhammad Shafiq[3], Aftab Ahmad Khan[1], Muhammad Muhitur Rahman[1]*

[1]Department of Civil and Environmental Engineering, College of Engineering, King Faisal University, Al-Ahs, Saudi Arabia
[2]Department of Agricultural Engineering, College of Food & Agriculture Sciences, King Saud University, Riyadh, Saudi Arabia
[3]Alamoudi Water Research Chair, King Saud University, Riyadh, Saudi Arabia

**Corresponding author: mqdir@kfu.edu.sa*

Citation: Amin M.T., Alazba A.A., Shafiq M., Khan A.A., Rahman M.M. (2026): Ca–Mg–Al LDH-modified wheat straw biochar for efficient lead chemisorption from aqueous solution: Insights from isotherm and kinetic analyses. Soil & Water Res., 21: 52–65.

Abstract: This study reports layered double hydroxides (LDHs) modified wheat straw biochar (W-B), denoted as (LDH/W-B), as an efficient adsorbent material for removal of lead (Pb^{2+}) ions from aqueous solution. This study also juxtaposes the adsorptive performance of LDH/W-B with W-B for Pb^{2+} removal. W-B was prepared via pyrolysis of wheat straw in a muffle furnace, using a controlled heating rate of 5 °C per min to reach 600 °C over a duration of three hours. Subsequently, LDH/W-B was synthesised using the co-precipitation method. Both resulting adsorbents were characterised for surface morphology and functional groups by means of scanning electron microscope (SEM) and Fourier transform infrared (FTIR), respectively. The influence of key adsorption parameters on the adsorption efficiency of W-B and LDH/W-B was systematically evaluated. At 60 min, the maximum Pb^{2+} removal efficiency was observed to be 78.21% for W-B and 92.4% for LDH/W-B. An increase in adsorbent dosage from 0.05 to 0.7 g and at a contact time of 1 h further enhanced Pb^{2+} removal, achieving efficiencies of 97% for W-B and 99% for LDH/W-B. The optimal conditions for maximum Pb^{2+} removal were determined to be 0.3 g of adsorbent (W-B and LDH/W-B), an initial heavy metal concentration of 10 mg/L, and a contact time of 1 h. Pb^{2+} removal data of W-B and LDH/W-B best fitted to the Langmuir isotherm and pseudo-second order kinetic model, which confirmed the dominance of chemisorption of Pb^{2+} ions. Additionally, the maximum theoretical adsorption capacity for Pb^{2+} is close to the experimentally obtained values, suggesting that the adsorption of Pb^{2+} primarily occurs through monolayer formation on the surface of both adsorbents. Overall, this study demonstrates that LDH/W-B is a highly promising adsorbent for Pb^{2+} removal in wastewater treatment applications.

Keywords: activated biochar; adsorption; layered double hydroxides; pseudo-second-order

Supported by he Deanship of Scientific Research, Vice Presidency for Graduate Studies and Scientific Research, King Faisal University, Saudi Arabia (Grant No. KFU254430). The authors extend their appreciation for the financial support that made this study possible.

https://doi.org/10.17221/106/2025-SWR

The increased level of hazardous elements pollution with rapid industrialisation presents serious threats to the environment, because of its high toxicity, long retention time, and the difficulty of repair (Zhang et al. 2020). Especially, heavy metals can enter the food chain and build up in the human body, resulting in irreversible physiological damage (Hu et al. 2016). Lead (Pb^{2+}) is a highly toxic heavy metal, contaminating the environment, posing serious risks to human health and ecosystems. Major sources of lead pollution include mining, battery manufacturing, smelting processes, and the pigment industry (Cheng & Hu 2010; Yang et al. 2021). Owing to its significant toxicity, lead can initiate serious harm to the immune system, resulting in issues like joint disorders, kidney failure, nervous system problems, and brain damage in foetuses (Argun et al. 2008). Due to the high toxicity of lead, removing lead ions from aqueous solutions is crucial to mitigate environmental and health risks. Various techniques have been employed for the elimination of heavy metal pollution, such as solvent extraction (Konczyk et al. 2016), chemical precipitation (Liao et al. 2019), and electrocoagulation (Peng & Guo 2020). Amongst these techniques, adsorption has been widely used because its cost-effectiveness, high efficiency, and simple procedure (Argun et al. 2008). The choice of adsorbent is crucial for maximising the efficiency of the adsorption process.

Biochar is a carbon-rich material crafted by pyrolysing biomass in environments with minimal oxygen or under anaerobic conditions (Chia et al. 2014). Biochar has been extensively utilised for the treatment of heavy metal pollution because of its large surface area, extensive porosity, and rich surface functional groups (Wei et al. 2022). Agricultural waste biomass is a valuable and renewable resource for biochar production, as its high lignin-to-cellulose ratio leads to a greater carbon yield, as stated by (Bhatnagar & Sillanpaa 2010). In a study, Sanka et al. (2020) synthesised biochar using rice husk and claimed to achieve a 90% removal efficiency for Pb^{2+} and various other heavy metals. The fine particle size of biochar complicates solid-liquid separation after adsorption, and its adsorption efficiency drops owing to the loss of functional groups during pyrolysis. To address these challenges, researchers are concentrating on developing biochar-based composites (Tan et al. 2016). Biochar is now utilised as a substrate in composites with advanced adsorbents, including graphene, carbon nanotubes (CNTs), metal organic framework (MOF), and layered double hydroxide (LDH). This combination greatly enhances the adsorption capacity compared to pristine biochar (Musarurwa & Tavengwa 2022).

LDH are types of metal hydroxide sheets that contain intercalated anions (like CO_3^{2-}, SO_4^{2-}, NO^{3-}, and Cl^-) along with interlayer water. The general formula for these compounds is:

$$[M_{1-x}^{2+}M_x^{3+}*(OH^-)_2]^{x+}(A^{n-})_{x/n}\cdot mH_2O$$

where M^{2+} and M^{3+} denotes to divalent (2^+) and trivalent (3^+) cation that are located on the sheets, while A^{n-} represents the intercalated anion (Tang et al. 2020). The exceptional characteristics of LDH, such as its high concentration of hydroxyl groups that facilitate the deposition of heavy metal ions, exceptional chemical and thermal stability, and significant capacity for intercalating various molecules, render it extremely effective for wastewater treatment (Mohapatra & Parida 2016). However, agglomeration during LDH preparation at the nanoscale reduces the specific surface area and active sites, thereby limiting its adsorption efficiency (Peligro et al. 2016). Recent studies indicate that biochar is effective in preventing particle aggregation and provides a high reactive surface area. When biochar is combined with LDHs, it overcomes the limitations of LDHs and enhances their synergetic ability to eliminate different contaminants from water (Vithanage et al. 2020; Liu et al. 2021). Ibrahim et al. developed a 3D nanoflower NiRu-LDH/Ti_4O_7 through a simple in situ growth method and found that the addition of Ti_4O_7 significantly reduced agglomeration (Ibrahim et al. 2018).

Recently, biochar-LDH (B-LDH) composite materials have shown considerable potential for enhancing pollutant removal. Numerous studies have explored the mechanisms of heavy metal adsorption employing biochar-supported LDH composites. For instance, Tan et al. (2022) synthesised a Zn-Fe-LDH and kiwi branch biochar (KB/Zn-Fe) composite for the efficient elimination of Pb^{2+} from water (Tan et al. 2022). They reported an adsorption capacity of 161.29 mg/g, which is significantly eminent than the 36.76 mg/g capacity of the original biochar. Jia et al. (2019) and Wang et al. (2018) developed a MnAl-LDH biochar composite for the efficient removal of Cu(II) ions, reaching a notable adsorption capacity of 74.04 mg/g. Khandaker et al. (2021) designed a composite using bamboo waste charcoal and MgFe-LDH for the removal of Cu(II) ions from contaminated water, achieving an adsorption capacity of 85.47 mg/g.

https://doi.org/10.17221/106/2025-SWR

However, studies on the simultaneous adsorption capacity and mechanism of biochar-supported LDHs for heavy metal removal remain limited.

In this study, raw wheat straw biochar (W-B) and a CaMgAl-LDH-modified W-B (LDH/W-B) composite were synthesised via a co-precipitation method to develop an efficient adsorbent for Pb(II) removal. Biomass-derived materials such as wheat straw are generally recognised in the literature as low-cost and sustainable precursors for sorbent production, due to their abundance and waste-based origin (Kurniawan et al. 2006; Gupta & Babu 2008; Li et al. 2025; Patel et al. 2025). The mechanisms involved in Pb^{2+} removal from aqueous solution were examined. Batch adsorption experiments were directed to weigh the impact of various operational parameters on lead adsorption efficiency. Additionally, different isotherm and kinetic models were utilised to assess the adsorption process.

MATERIAL AND METHODS

Biochar preparation. Wheat straws were obtained from King Saud University in Riyadh, located in the rural area of Drab, near Riyadh city, Saudi Arabia. The straws were washed, dried, and then crushed into small pieces. These pieces were sieved using a 0.3 mm sieve to separate them. The resulting material was slowly pyrolysed in a box muffle furnace (Nabertherm, B-150, Germany) set to a temperature increase of 5 °C per min for three hours at 600 °C. The obtained biochar, termed as W-B, was rinsed with distilled water to eliminate ash, and subsequently dried out in a furnace at 105 °C for 8 hours. Later, it was stored in the desiccator till applied in experiments.

CaMgAl-LDH and W-Biochar composite. The co-precipitation method was employed to make the CaMgAl-LDH/W-Biochar composite adsorbent. To prepare CaMgAl-LDH, 5.90 g (0.5 M) of calcium nitrate tetrahydrate ($Ca(NO_3)_2{\cdot}4H_2O$), 6.025 g (0.5 M) of aluminium nitrate nonahydrate ($Al(NO_3)_3{\cdot}9H_2O$), and 6.41 g (0.5 M) of magnesium nitrate hexahydrate ($Mg(NO_3)_2{\cdot}6H_2O$) were dissolved in 50 mL of distilled water with continuous stirring for one hour to confirm complete dissolution. The solution was then added to a separate beaker containing 5 g of W-Biochar while stirring continuously. A prepared solution of 0.42 g NaOH and 0.58 g Na_2CO_3 in 100 mL of water was steadily added using a burette until the pH reached around 10. The mixture was stirred for another two hours before being centrifuged at 6 000 rpm to separate the solid phase. This washing process was repeated five times using deionised water. Finally, synthesised composite dried out in a furnace at 85 °C for 24 hours.

Batch adsorption experiment. All adsorption experiments were conducted under controlled batch conditions at room temperature (25 ± 1 °C). W-B and LDH/W-B were added to capped volumetric flasks, filled with a Pb^{2+} solution during batch adsorption experiments. Stock solution of 30 ppm was prepared for lead. For each experiment, an appropriate dose of both W-B LDH/W-B adsorbents was added to 40 mL of the metal ion solution in a flask (0.3 g/L for W-B and 0.4 g/L for LDH/W-B). The solution pH was set to 6 using 0.1 M HCl and NaOH as needed. The flasks were shaken at 220 rpm in a Wise Cube orbital shaker (Daihan Scientific Co. Ltd, Wisd. ThermoStable IS-20, South Korea). After adsorption the samples were centrifuged (Hermle Z 400 K, Germany) at 6 000 rpm for 15 min, and the Pb^{2+} concentration in the supernatant was analysed using a flame atomic absorption spectrometry (FAAS, Thermo Scientific, ICE 3000 Series, Cambridge, UK) at maximum absorption wavelength of lead i.e., 283 nm.

The effect of pH (2–6), W-B and LDH/W-B (0.05 to 0.7 g) dosage, initial concentration of Pb^{2+} (10 to 60 mg/L), and 120 min contact time was investigated. The removal efficiency (%) and Pb^{2+} uptake (q_e) were measured by the following equations, respectively.

$$\text{Removal}(\%) = \left(\frac{C_i - C_e}{C_i}\right)100 \quad (1)$$

$$q_e = \left(\frac{C_i - C_e}{m}\right)v \quad (2)$$

where:

C_e – the equilibrium concentration of Pb^{2+} (mg/L);

C_i –the initial concentration of Pb^{2+} (mg/L);

m – mass of adsorbent (g);

v – volume of the solution (L).

Calibration curves ($R^2 > 0.999$) were prepared using freshly prepared $Pb(NO_3)_2$ standards (0.5–10 mg/L). Analytical blanks and standard reference samples were measured after every ten readings to verify instrument stability. All glassware was acid-washed (10% HNO_3) and rinsed with deionised water before use to minimise contamination. Each adsorption experiment was conducted in triplicate, and results are reported as mean ± standard deviation.

https://doi.org/10.17221/106/2025-SWR

Characterisation techniques. Both W-B and LDH/W-B samples were characterised using various characterisation techniques such as Fourier transform infrared (FTIR) spectroscopy (VERTEX 70v vacuum spectrometer, Bruker, USA) in the wavenumber range of 4 000–400 cm^{-1}, using KBr pellets with a spectral resolution of 4 cm^{-1}. Surface morphology was examined using a Scanning electron microscope (SEM; HITACHI S–3000N, Japan) equipped with an Oxford Instruments Energy-Dispersive X-ray (EDX) detector operated at an accelerating voltage of 15 kV. Prior to SEM imaging, samples were sputter-coated with a thin layer of gold (≈ 10 nm) to prevent surface charging. FTIR analysis was used to recognise the chemical bonds and functional groups (Haleem et al. 2022) present on the W-B and LDH/W-B surface of the adsorbents, both before and after Pb^{2+} adsorption. SEM and Energy Dispersive EDX specified some insights into the surface morphology (Obey et al. 2022), revealing the structural changes and the adsorption of metal ions, which helped assess the effectiveness of both W-B and LDH/W-B in removing Pb^{2+} from aqueous solutions. All analytical instruments were calibrated prior to measurement to ensure data accuracy.

RESULT AND DISCUSSION

Fourier transform infrared spectroscopy (FTIR)

The FTIR spectra of W-B (Figure 1A) shows characteristic peaks at 2 119 cm^{-1}, indicating the presence of C≡C or C≡N stretching vibrations, which suggest unsaturated alkyne or nitrile groups. A peak at 1 417 cm^{-1} corresponds to C-H bending or aromatic C=C stretching, implying the aromatic structure of the biochar (Behazin et al. 2015). The band at 1 021 cm^{-1} is attributed to the C-O stretching vibrations from cellulose, hemicellulose, and lignin. Meanwhile, the bands at 875 and 791 cm^{-1} correspond to the aromatic C-H bending and ring deformation, respectively (Liu et al. 2015). After Pb^{2+} adsorption (Figure 1B), the FTIR spectrum has changed with the appearance of a peak at 2 089 cm^{-1} and shift or disappearance of other peaks, indicating interactions between Pb ions and the functional groups on the surface of biochar. Figure 1C shows the LDH/W-B spectra. The broad band observed at 3 384 cm^{-1} corresponds to the vibrational hydroxyl group, while a short shoulder peak at 1 620 cm^{-1} is assigned to H_2O (Xu et al. 2020). The characteristic peaks at 2 093 cm^{-1}, indicates C≡C or C≡N stretching vibrations, suggesting unsaturated

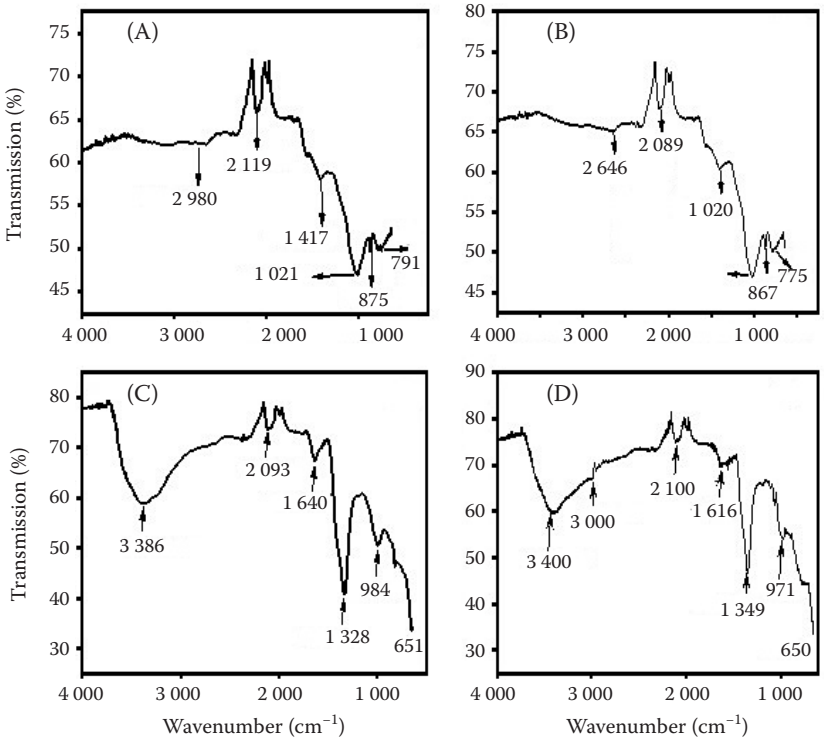

Figure 1. Fourier transform infrared (FTIR) spectra of W-B (A), W-B after Pb^{2+} adsorption (B), LDH/W-B (C), and LDH/W-B after Pb^{2+} adsorption (D)

W-B – raw wheat straw biochar; LDH – layered double hydroxide

https://doi.org/10.17221/106/2025-SWR

alkyne or nitrile groups. The sharp peaks at 1 328 and 984 cm^{-1} were attributed to the asymmetric stretching vibration mode of C-O in CO_3^{2-} and stretching of C-O respectively (Adachi-Pagano et al. 2003; Zou et al. 2017). The peak at 650 cm^{-1} relates to the lattice bending vibrations of M-OH or M-O groups (Lyu et al. 2023). The FTIR spectrum of LDH/W-B after lead adsorption of Pb^{2+} is shown in Figure 1D, all the peaks were shifted to higher wavelength after lead adsorption. The OH band was narrowed down after lead adsorption. This variation confirmed the successful adsorption of Pb^{2+} on LDH/W-B, mediated through its surface functional groups.

Scanning electron microscopy

It is commonly used for characterising biochar and is valuable in detecting macro-pores within the biochar structure. It grants valuable intuitions into the ultimate composition and surface morphology of biochar, revealing its textural features at high resolution (Amin et al. 2016). The SEM image of W-B and LDH/W-B in Figures 2A and 2C represents a porous morphology with a honeycomb-like structure characterised by interconnected holes. The surface of W-B contains many well-defined pores evenly distributed across it and forming a nice and symmetrical pattern. The surface displays vesicle-like features whereby some of the larger holes are interconnected with smaller ones to form net-like structures that enhance the material's structural complexity. Both W-B and LDH/W-B display a regular arrangement of perpendicular blocks, further highlighting its complex microstructure (Wang et al. 2024). The SEM images suggest that the LDH/W-B contains higher pore volume with deeper and wider cylindrical holes, suggesting its suitability for enhanced adsorption. SEM images of W-B and LDH/W-B in Figures 2B and 2C after Pb^{2+} adsorption exhibit notable changes in surface morphology compared to the pristine biochar. The well-defined pores and cylindrical structures now appear partially or filled, indicative of successful metal-ion adsorption. Honeycomb-like

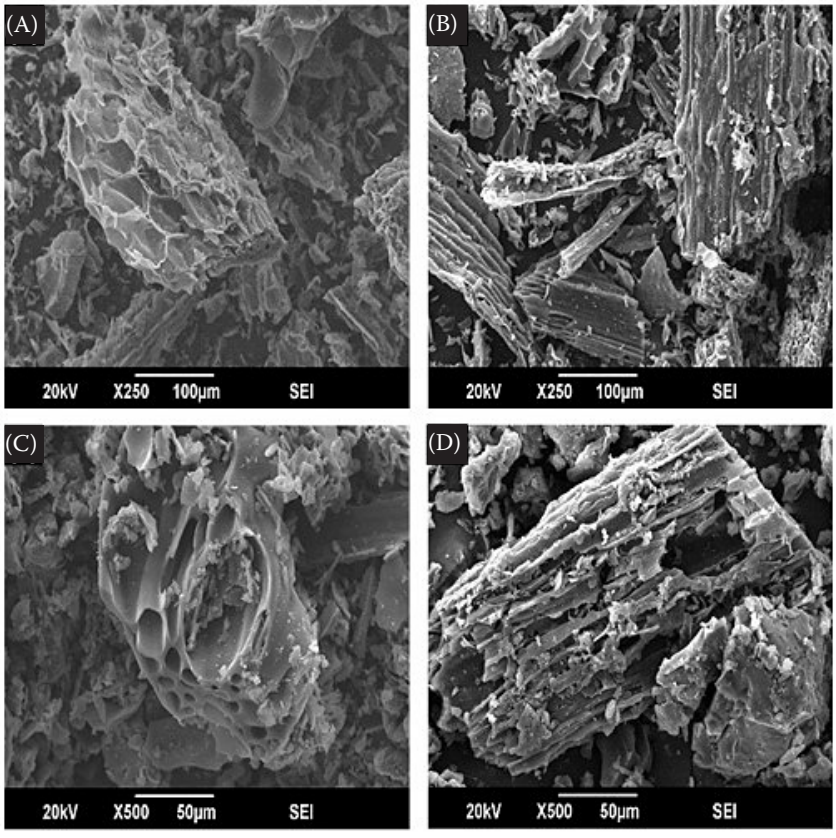

Figure 2. Scanning electron microscope (SEM) images of W-B (A), W-B after Pb^{2+} adsorption (B), LDH/W-B (C), and LDH/W-B after Pb^{2+} adsorption (D)

W-B – raw wheat straw biochar; LDH – layered double hydroxide; SEI – secondary electron imaging

https://doi.org/10.17221/106/2025-SWR

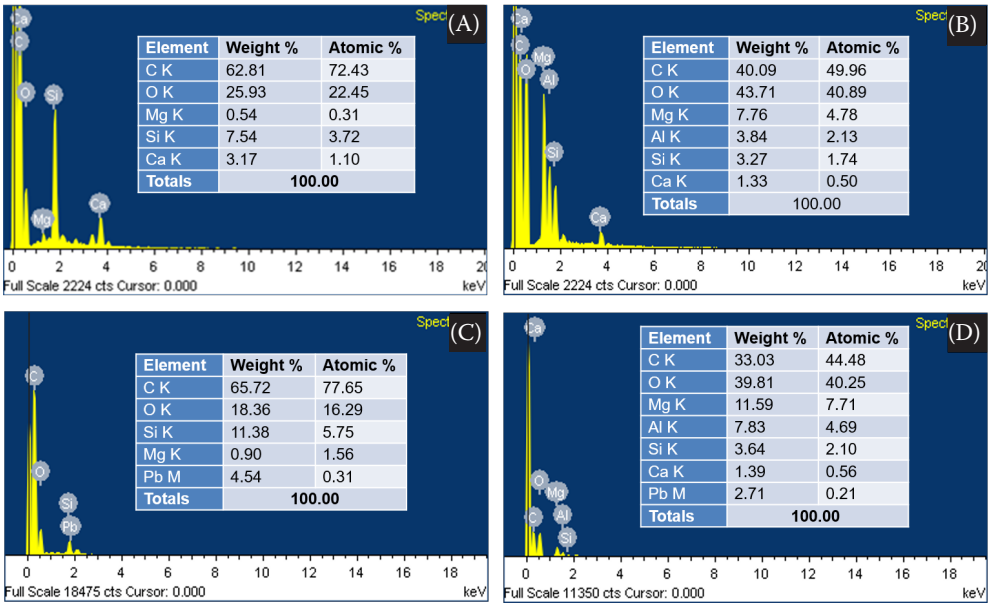

Figure 3. Energy-dispersive X-ray (EDX) of W-B (A), LDH/W-B (B), W-B after Pb^{2+} adsorption (C), and LDH/W-B after Pb^{2+} adsorption (D)

W-B – raw wheat straw biochar; LDH – layered double hydroxide

structures are less pronounced, with pores seemingly blocked by adsorbed Pb^{2+} particles. However, the surface appears rougher and more irregular in the case of LDH/W-B, suggesting the enhanced accumulation of metal ions on the surface. These observations confirm that LDH/W-B is more efficient in absorbing heavy metals from aqueous solutions.

The EDX analysis in Figures 3A–D validates the elemental composition and surface properties of the biochar and CaAlMg(LDH)-biochar before and after Pb^{2+} adsorption. The minerals content in W-S biochar as carbon, oxygen, and silicate were considered an important characteristic for biochar (Zaitun et al. 2022). The W-S biochar has a high C and O content, whereas CaAlMg(LDH)-biochar contains extra elements such as Mg, Al, Si, and Ca due to the formation of layered double hydroxides (LDH). After Pb^{2+} adsorption, both W-B and LDH/W-B show a substantial Pb^{2+} peak, indicating that Pb^{2+} was successfully removed. The LDH/W-B demonstrates enhanced Pb^{2+} adsorption compared to W-B, which can be attributed to higher active site availability and adsorption capacity.

Impact of process variables on the adsorption of Pb^{2+} onto W-B and LDH/W-B

To thoroughly investigate the adsorption process, variables including contact time, solution pH, dose of adsorbent and initial dye concentration must be considered to evaluate their impact on adsorption efficiency.

Influence of contact time. The influence of contact time is a crucial factor in the determination of the adsorption kinetics. The adsorption of Pb^{2+} onto W-B and LDH/W-B was examined over different time intervals (1, 5, 10, 15, 30, 60, 100 and 180 min), while keeping the concentration (30 mg/L) and dose (0.3 g) constant at solution pH 6. Figure 4 illustrates that the removal efficiency of lead onto both adsorbents increased consistently during the first 60 min of the experiment, with the removal efficiency of 78.68% for W-B (Figure 3A) and 92.4% for LDH/W-B (Figure 4B). This can be ascribed to the availability of the unoccupied available sites on the composite. However, from 60 to 180 min, there is little to no change in the Pb^{2+} removal efficiency, owing to the fact that Pb^{2+} ions had already occupied the available adsorption sites (Jeyakumar & Chandrasekaran 2014). This indicates that adsorption equilibrium is reached within the initial 60 minutes. Further experiments were performed within 60 minutes.

Effect of adsorbents dose. The study employed doses of both W-B and LDH/W-B ranging from 0.05 to 0.7 g, keeping all other parameters constant. As the dosage of the adsorbent increases from 0.05 to 0.7, the uptake of Pb^{2+} increases, reaching a maximum

https://doi.org/10.17221/106/2025-SWR

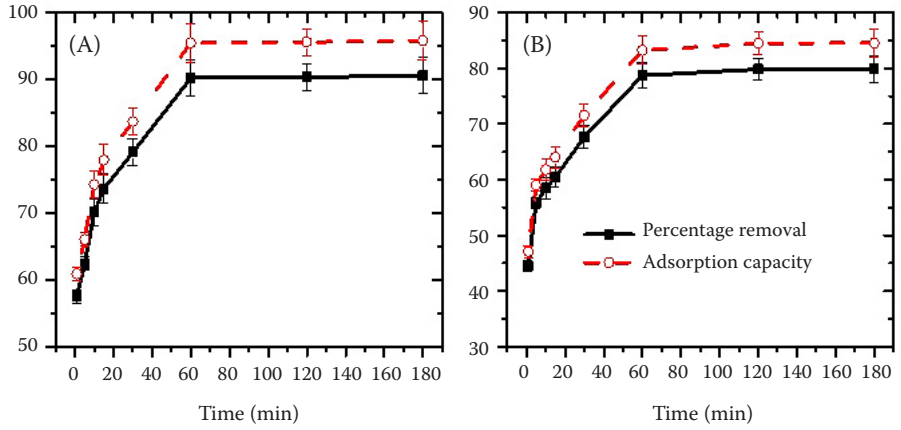

Figure 4. Effect of contact time on the adsorption capacity (in mg/g) and percentage removal of Pb^{2+} from aqueous solutions onto W-B (A) and LDH/W-B (B)
W-B – raw wheat straw biochar; LDH – layered double hydroxide

removal efficiency of 97 and 99% at an adsorbent dose of 0.7 g for both W-B and LDH/W-B, as shown in Figure 5. However, for practical and economic considerations, an optimised adsorbent dose of 0.3 g was selected, as it achieved 78 and 90.2% removal for both W-B and LDH/W-B. Increasing the doses beyond 0.3 g resulted in only marginal improvements, with a 9% increase in removal efficiency up to 99.9% at 0.7 g. Therefore, 0.3 g was deemed the optimal dose, balancing high removal efficiency with cost-effectiveness. Hence, 0.3 g was selected as the optimum adsorbent dosage for the removal of Pb metal ions and for further investigation in this study.

Effect of initial concentration of Pb^{2+}. Figure 6 shows the change in adsorption efficiency with changed initial concentrations, varying from 10 to 60 mg/L for W-B and LDH/W-B, respectively. Throughout the experiment, the pH (6), contact time (60 min), adsorbent dosage (0.3 g), and temperature (25 °C) were kept constant. Removal efficiency was decreased in both cases with an increase in initial concentration, with a maximum removal of 95% for W-B and 99% for LDH/W-B at 10 mg/L. The decline in the percentage removal of metal can be ascribed to the augmented Pb metal ions in the aqueous phase, causing competition and saturation on the adsorbent surface. This, in turn, hinders mass transfer (El-Shafey et al. 2024).

Effect of pH. The pH of the solution plays a crucial role in adsorption, as it affects the surface charge of the adsorbent and the dissociation of its functional groups. Additionally, pH influences the ionisation state and speciation of metal ions. Thus,

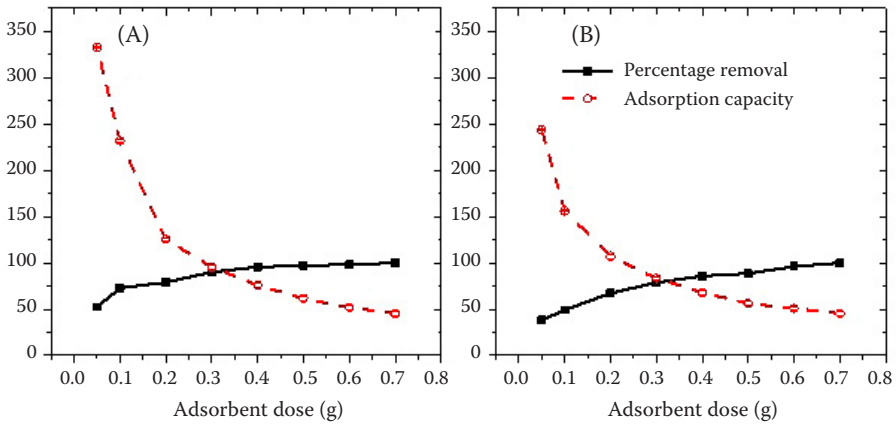

Figure 5. Effect of W-B (A) and LDH/W-B (B) dose on the adsorption capacity (mg/g) and percentage removal of Pb^{2+}
W-B – raw wheat straw biochar; LDH – layered double hydroxide

https://doi.org/10.17221/106/2025-SWR

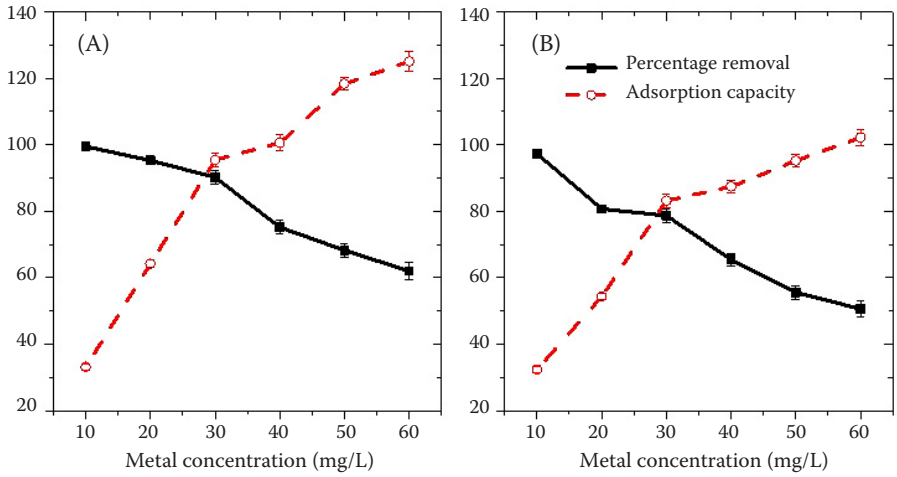

Figure 6. Effect of Pb^{2+} concentrations on the adsorption capacity (mg/g) and percentage removal using W-B (A) and LDH/W-B (B) as an adsorbent

W-B – raw wheat straw biochar; LDH – layered double hydroxide

Pb ions adsorption onto both W-B and LDH/W-B was studied in the pH range of 2 to 6. The results shown in Figure 7 clearly indicate that the removal of Pb^{2+} was significantly influenced by pH, with the removal efficiency increasing from 7 to 78% for W-B (Figure 6A) and 9 to 90% for LDH/W-B (Figure 6B), as the initial pH increased from 2.0 to 6.0. Under strongly acidic conditions, the high concentration of H^+ ions leads to the protonation of the adsorbents surface, making it positively charged. This positive charge creates electrostatic repulsion, which hinders metal ions from getting close to the surface, resulting in reduced removal efficiency at low pH values. Conversely, as the pH of the solution increases, the adsorption sites on the adsorbents gain a negative charge, facilitating the adsorption of more metal ions as the pH rises (Reddy & Lee 2014).

Adsorption kinetics

To understand the mechanism of adsorption of Pb^{2+} onto both W-B and LDH/W-B, the experimental kinetic data were analysed using the pseudo-first order (PFO), pseudo-second order (PSO), and intra-particle diffusion models (IPD), as shown in Figure 8.

The PFO model indicates that the rate at which the solute is taken up is proportional to the difference between the saturation concentration and the total of adsorbate that has accumulated on the adsorbent

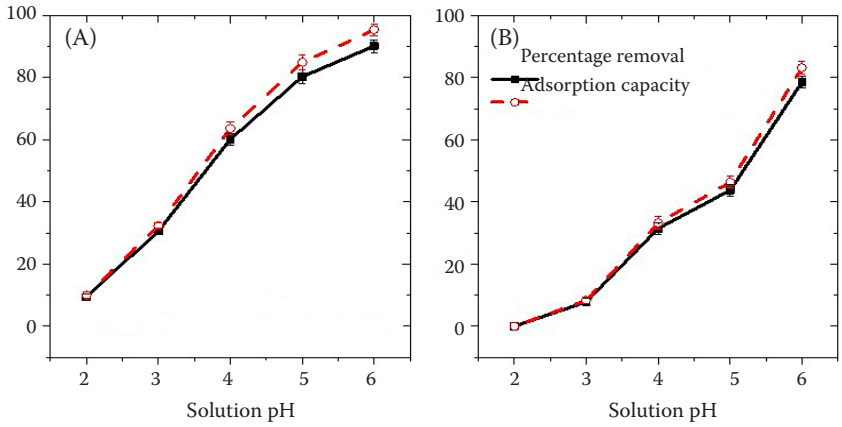

Figure 7. Effect of pH on the adsorption capacity (mg/g) and percentage removal of Pb^{2+} using W-B (A) and LDH/W-B (B) as adsorbent

W-B – raw wheat straw biochar; LDH – layered double hydroxide

https://doi.org/10.17221/106/2025-SWR

Table 1. Kinetic model parameters for the adsorption of Pb^{2+} on the surface of both W-B and LDH/W-B adsorbents

Kinetic models	Parameters	W-B	LDH/W-B
PFO	K_1	0.03	0.04
	q_{exp}	83.25	95.40
	q_{cal}	32.51	33.54
	R^2	0.941	0.962
PSO	K_2	0.11	0.0037
	q_{cal}	83.33	100
	R^2	0.992	0.994
IPD	I	44.87	56.32
	k_{diff}	4.91	5.12
	R^2	0.975	0.987

PFO – pseudo-first order; PSO – pseudo-second order; IPD – intra-particle diffusion models; W-B – raw wheat straw biochar; LDH – layered double hydroxide

over time. This model is generally relevant during the early stages of the adsorption procedure. In contrast, the PSO model posits that chemisorption is the rate-limiting step and is applicable throughout the entire adsorption procedure.

The linear expressions for the PFO and PSO models are expressed in Equation (3) and Equation (4), respectively (Ho & McKay 1998; Lagergren 1898).

$$\log(q_e - q_{t)} = \log q_e - \frac{k_1}{2.303}t \quad (3)$$

$$\frac{t}{q_t} = \frac{1}{k_2 q_e^2} + \frac{t}{q_t} \quad (4)$$

where:

k_1, k_2 – the rate constants for the PFO and PSO kinetic models measured in min^{-1} and g (mg/ min);

q_e – equilibrium adsorption capacity;

q_t – adsorption capacity at any specific time t.

Table 1 contains the constants and correlation coefficients calculated for both kinetic models.

Correlation coefficient R^2 for PFO (0.941for W-B and 0.962 for LDH/W-B) are lower than PSO (0.992 for W-B and 0.994 for LDH/W-B) and the calculated q_e value of PSO model are in good agreement with the experimental values while calculated q_e values

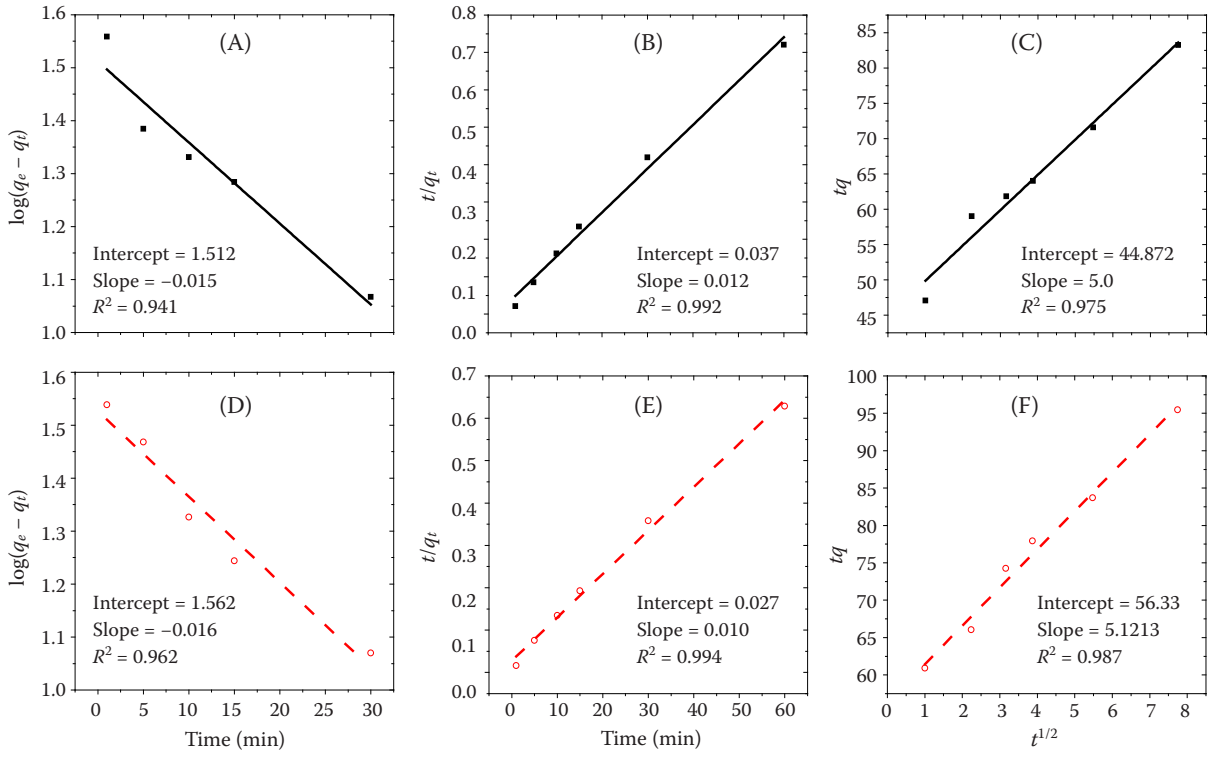

Figure 8. Pseudo-first order (PFO) (A, D), pseudo-second order (PSO) (B, E), and intra-particle diffusion models (IPD) (C, F) kinetic model analysis for both W-B and LDH/W-B, respectively

W-B – raw wheat straw biochar; LDH – layered double hydroxide

https://doi.org/10.17221/106/2025-SWR

of PFO significantly disagree from experimental value for both the adsorbents. These results indicate that the adsorption kinetics obeyed the PSO model which in turn indicates the chemical adsorption as the rate limiting step in both cases.

Kinetic data were further examined, to understand the diffusion mechanism, using Weber's IPD, which can be defined as (Weber & Morris 1963):

$$q_t = k_{ip} t^{1/2} + C \quad (5)$$

where:

C – the thickness of the boundary layer;

k_{ip} – intraparticle diffusion rate constant.

Higher C values indicate a stronger impact of the boundary layer. The results show a strong alignment between the kinetic data for Pb^{2+} and the IPD model, with R^2 values of 0.975 for W-B and 0.986 for LDH/W-B (Table 1). This indicates that as compared to other diffusion processes, the IPD process is the primary rate-controlling step in the adsorption of Pb^{2+} onto both adsorbents. This conclusion is further reinforced by the observation that the linear plot of (q_t) versus ($t^{0.5}$) does not pass through the origin, which emphasises the role of boundary layer diffusion during the adsorption. Moreover, the positive C value supports the idea that IPD is involved in the adsorption process, however, the adsorption process is not solely governed not only by IPD as the rate-limiting step; other factors also influence Pb^{2+} adsorption on both W-B and LDH/W-B composite (Al-Musawi et al. 2022).

Adsorption isotherms

The adsorption for the removal of Pb^{2+} using both W-B and LDH/W-B adsorbents was assessed by Langmuir, Freundlich, and Temkin models as shown in Figure 9. The Langmuir isotherm describes the adsorption process in which a single layer of adsorbate forms on a surface, with no interactions occurring between the adsorbate molecules (Hussain et al. 2025). In contrast, the Freundlich isotherm is often used for heterogeneous solid catalysts and serves as a mathematical model for multilayer adsorption. The Temkin isotherm, however, considers adsorption in heterogeneous systems, proposing that the heat of adsorption decreases linearly as surface coverage increases, due to the interactions between the adsorbent and adsorbate. It also implies that the binding energies of the adsorbates are evenly distributed.

The linear expression of the Langmuir isotherm, which assumes single-layer adsorption, is represented by Equation (6) (Langmuir 1918). Similarly, the linear forms of the Freundlich isotherm and the Temkin isotherm are described by Equation (7) (Agarwal et al. 2016) and Equation (8) (Temkin & Pyzhev 1940), respectively.

$$\frac{1}{q_e} = \frac{1}{K_L q_{\max}} + \frac{C_e}{q_{\max}} \quad (6)$$

$$\log q_e = \log K_F + \frac{1}{n} \log C_e \quad (7)$$

$$q_e = \frac{RT}{B_T} \ln A_T + \frac{RT}{B_T} \ln C_e \quad (8)$$

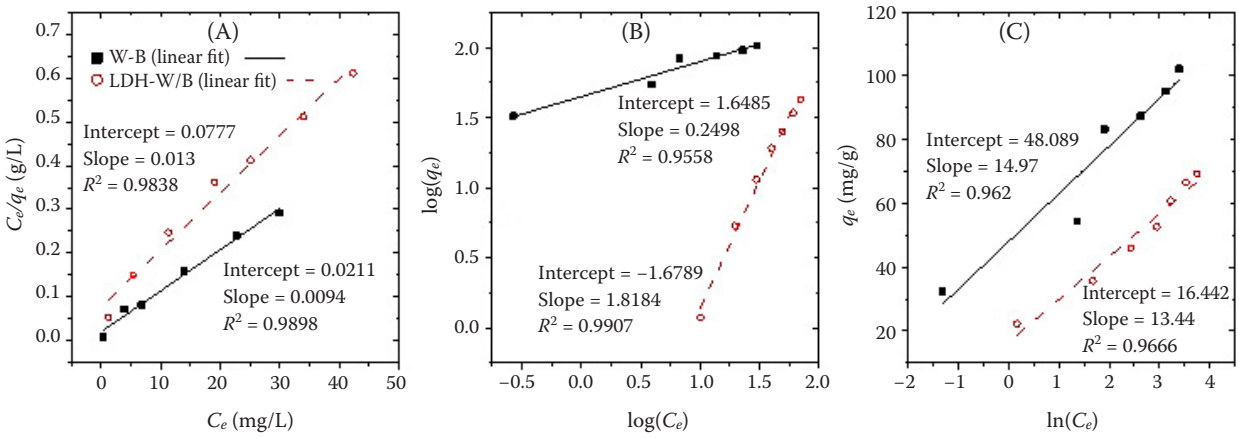

Figure 9. Adsorption isotherms: Langmuir isotherm (A), Freundlich isotherm (B), and Temkin isotherm (C) for Pb^{2+} adsorption on W-B and LDH/W-B

W-B – raw wheat straw biochar; LDH – layered double hydroxide

https://doi.org/10.17221/106/2025-SWR

where:
C_e – the equilibrium concentration of the dye solution (mg/L);
q_{max} – the maximum adsorption capacity (mg/g);
K_L – the equilibrium adsorption constant (L/mg);
K_F – the adsorption driving force (L/mg);
$1/n$ – the extent of non-linearity between adsorption and solution concentration;
A_T – the equilibrium binding constant associated with the maximum binding energy (L/mg);
RT – the product of universal gas constant (R) and absolute temperature (T);
B – constant relates to the heat of adsorption.

The fitting plots for these models are presented in Figure 9 for both W-B and LDH/W-B. Table 1 summarises the calculated parameters and correlation coefficients for the adsorption of Pb^{2+} onto both W-B and LDH/W-B adsorbents.

The Langmuir isotherm model indicates that the maximum theoretical adsorption capacities are in close agreement with the experimentally calculated values for W-B (q_{max} 126 and q_{exp} 125 mg/g) and LDH/W-B (q_{max} 111 and q_{exp} 102 mg/g) for Pb^{2+} adsorption. According to the Freundlich isotherm model, $1/n$ values indicate the type of isotherm as irreversible process ($1/n = 0$), a favourable process ($1/n < 1$), and an unfavourable process ($1/n > 1$). For favourable adsorption conditions, the value of n should be between 1 and 10. The Freundlich constant n values were 4.01(W-B) and 4.62 (LDH/W-B) for Pb^{2+}, indicating a favourable adsorption process (Table 2). According to the Temkin isotherm model, a higher value of B indicates a strong interaction force between the adsorbate and the adsorbent. The R^2 values of the Freundlich isotherm model (0.955 for W-B and 0.980 for LDH/W-B) and Temkin model (0.925 for W-B and 0.970 for LDH/W-B) models were lower than those obtained from the Langmuir isotherm model i.e., 0.969 and 0.991 for W-B and LDH/W-B, respectively. Additionally, the Langmuir isotherm model indicates that the maximum theoretical adsorption capacity for Pb^{2+} is close to the experimentally obtained value, suggesting that the adsorption of Pb^{2+} primarily occurs through monolayer formation in both cases.

Table 2. Isotherm model parameters of Pb^{2+} adsorption on surface of both W-B and LDH/W-B adsorbents

Isotherm models	Parameters	W-B	LDH/W-B
Langmuir	q_{exp}	102.21	126.42
	q_{max}	111.11	125.07
	R_L	0.02	0.008
	R^2	0.969	0.991
Freundlich	K_F	44.46	65.01
	N	4.01	4.62
	R^2	0.955	0.980
Temkin	B	1.96	15.22
	$Ln(A_T)$	3.21	4.85
	R^2	0.925	0.970

W-B – raw wheat straw biochar; LDH – layered double hydroxide

In the Langmuir model, R_L is a dimensionless constant separation factor, given by:

$$R_L = \frac{1}{1 + K_L C_o}$$

where:
K_L – Langmuir adsorption constant;
C_o – initial metal concentration.

The calculated R_L value between 0 and 1 for Pb^{2+} in both cases indicates favourable adsorption ($0 < RL < 1$) under the optimised conditions (Duran et al. 2011).

CONCLUSION

The study revealed the usefulness of both W-B and LDH/W-B as environmentally friendly adsorbents for the removal of heavy metals, particularly $Pb^{2+,}$ from aqueous solutions. The biochar was synthesised through pyrolysis at 600 °C with a controlled temperature increase of 5 °C per min and LDH/W-B was prepared by co-precipitation method. SEM and FTIR characterisation confirmed both W-B and LDH/W-B as appropriate materials for adsorption applications. SEM analysis showed a highly porous surface morphology with cylindrical holes and vesicle-like features for LDH/W-B that facilitate heavy metal adsorption. After Pb^{2+} adsorption, the pores appeared partially blocked, indicating successful adsorption. FTIR analysis identified functional groups such as hydroxyl (-OH), carbonyl (-C=O), and carboxyl (-COOH) on the adsorbent's surface, which play a key role in binding metal ions. The changes in FTIR peaks after adsorption were also supported by the chemical interaction between these groups and metal ions. Contact time, adsorbent dose, pH, and metal

https://doi.org/10.17221/106/2025-SWR

ion concentration affected the performance of both W-B and LDH/W-B. At the optimum conditions, that is, a dose of 0.3 g for both W-B and LDH/W-B, a Pb^{2+} concentration of 10 mg/L, and a contact time of 60 min, the maximum Pb^{2+} removal efficiency was found to be 78% for W-B and 92.4% for LDH/W-B. Adsorption isotherm study showed that adsorption of Pb^{2+} was in Langmuir, indicating monolayer adsorption, for both adsorbents. Kinetic study indicated that adsorption of Pb^{2+} was in accordance with the PSO model; therefore, the dominant mechanism might be chemisorption. These findings suggest that the removal efficiency of LDH/W-B is higher than W-B, suggesting the LDH/W-B as a cost-effective and eco-friendly solution for removal of heavy metals from wastewater. It could be produced in a sustainable process and with high adsorption capacity, which will make it promising for large-scale water treatment applications, thus presenting a better way to address environmental pollution.

Data availability. The data supporting the current study are available from the corresponding author upon request.

REFERENCES

Adachi-Pagano M., Forano C., Besse J.-P. (2003): Synthesis of Al-rich hydrotalcite-like compounds by using the urea hydrolysis reaction – control of size and morphology. Journal of Materials Chemistry, 13: 1988–1993.

Agarwal A.K., Kadu M.S., Pandhurnekar C.P., Muthreja I.L. (2016): Brunauer-Emmett-Teller (B.E.T.), Langmuir and Freundlich isotherm studies for the adsorption of nickel ions onto coal fly ash. Asian Journal of Water, Environment and Pollution, 13: 49–53.

Al-Musawi T.J., Mengelizadeh N., Al Rawi O., Balarak D. (2022): Capacity and modeling of acid blue 113 dye adsorption onto chitosan magnetized by Fe_2O_3 nanoparticles. Journal of Polymers and the Environment, 30: 344–359.

Amin F.R., Huang Y., He Y., Zhang R., Liu G., Chen C. (2016): Biochar applications and modern techniques for characterization. Clean Technologies and Environmental Policy, 18: 1457–1473.

Argun M.E., Dursun S., Karatas M., Gürü M. (2008): Activation of pine cone using Fenton oxidation for Cd(II) and Pb(II) removal. Bioresource Technology, 99: 8691–8698.

Behazin E., Ogunsona E., Rodriguez-Uribe A., Mohanty A.K., Misra M., Anyia A.O. (2015): Mechanical, chemical, and physical properties of wood and perennial grass biochars for possible composite application. BioResources, 11: 1334–1348.

Bhatnagar A., Sillanpaa M. (2010): Utilization of agro-industrial and municipal waste materials as potential adsorbents for water treatment – A review. Chemical Engineering Journal, 157: 277–296.

Cheng H., Hu Y. (2010): Lead (Pb) isotopic fingerprinting and its applications in lead pollution studies in China: A review. Environmental Pollution, 158: 1134–1146.

Chia C.H., Singh B.P., Joseph S., Graber E.R., Munroe P. (2014): Characterization of an enriched biochar. Journal of Analytical and Applied Pyrolysis, 108: 26–34.

Duran C., Ozdes D., Gundogdu A., Senturk H.B. (2011): Kinetics and isotherm analysis of basic dyes adsorption onto almond shell (*Prunus dulcis*) as a low cost adsorbent. Journal of Chemical & Engineering Data, 56: 2136–2147.

El-Shafey S.E., Obada M.K., El-Shamy A.M., Mohamed W.S. (2024): Silica/klucel nanocomposite as promising durable adsorbent for lead removal from industrial effluents. Scientific Reports, 14: 26095.

Gupta S., Babu B.V. (2008): Economic feasibility analysis of low cost adsorbents for the removal of Cr (VI) from wastewater. In: Proc. Int. Convention on Water Resources Development and Management (ICWRDM), BITS Pilani, Citeseer, 23–26.

Haleem N., Khattak A., Jamal Y., Sajid M., Shahzad Z., Raza H. (2022): Development of poly vinyl alcohol (PVA) based biochar nanofibers for carbon dioxide (CO_2) adsorption. Renewable and Sustainable Energy Reviews, 157: 112019.

Ho Y.S., McKay G. (1998): Sorption of dye from aqueous solution by peat. Chemical Engineering Journal, 70: 115–124.

Hu S., Su Z., Jiang J., Huang W., Liang X., Hu J., Chen M., Cai W., Wang J., Zhang X. (2016): Lead, cadmium pollution of seafood and human health risk assessment in the coastline of the southern China. Stochastic Environmental Research and Risk Assessment, 30: 1379–1386.

Hussain N., Asif M., Shafaat S., Khan M.S., Riaz N., Iqbal M., Javed A., Butt T.A., Shaikh A.J., Bilal M. (2025): Multilayer adsorption of reactive orange 16 dye onto Fe_2O_3/ZnO hybrid nanoadsorbent: Mechanistic insights from kinetics, isotherms and dynamic light scattering studies. Journal of Chemical Technology & Biotechnology, 100: 50–66.

Ibrahim K.B., Su W.-N., Tsai M.-C., Chala S. A., Kahsay A.W., Yeh M.-H., Chen H.-M., Duma A.D., Dai H., Hwang B.-J. (2018): Robust and conductive Magnéli Phase Ti_4O_7 decorated on 3D-nanoflower NiRu-LDH as high-performance oxygen reduction electrocatalyst. Nano Energy, 47: 309–315.

Jeyakumar R.P.S., Chandrasekaran V. (2014): Adsorption of lead (II) ions by activated carbons prepared from marine green algae: equilibrium and kinetics studies. International Journal of Industrial Chemistry, 5: 10.

https://doi.org/10.17221/106/2025-SWR

Jia Y., Zhang Y., Fu J., Yuan L., Li Z., Liu C., Zhao D., Wang X. (2019): A novel magnetic biochar/MgFe-layered double hydroxides composite removing Pb^{2+} from aqueous solution: Isotherms, kinetics and thermodynamics. Colloids and Surfaces A: Physicochemical and Engineering Aspects, 567: 278–287.

Khandaker S., Hossain M.T., Saha P.K., Rayhan U., Islam A., Choudhury T.R., Awual Md.R. (2021): Functionalized layered double hydroxides composite bio-adsorbent for efficient copper(II) ion encapsulation from wastewater. Journal of Environmental Management, 300: 113782.

Konczyk J., Nowik-Zajac A., Kozlowski C.A. (2016): Calixarene-based extractants for heavy metal ions removal from aqueous solutions. Separation Science and Technology, 51: 2394–2410.

Kurniawan T.A., Chan G.Y., Lo W.H., Babel S. (2006): Comparisons of low-cost adsorbents for treating wastewaters laden with heavy metals. Science of the Total Environment, 366: 409–426.

Lagergren S. (1898): About the theory of so-called adsorption of soluble substances. Kungliga Svenska Vetenskapsakademiens Handlingar, 24: 1–39.

Langmuir I. (1918): The adsorption of gases on plane surfaces of glass, mica and platinum. Journal of the American Chemical Society, 40: 1361–1403.

Li Z. Lu G., Du D., Zhao D. (2025): Harnessing low-cost adsorbents for removal of heavy metals and metalloids in contaminated water: Progress in the past decade and future perspectives. Journal of Cleaner Production, 518: 145845.

Liao W., Zhao Q., Chen H., Liao C., Wang Y., Wang X. (2019): Experimental investigation and simulation optimization of a pilot-scale supercritical water oxidation system. Energy Conversion and Management, 199: 111965.

Liu R., Wang H., Han L., Hu B., Qiu M. (2021): Reductive and adsorptive elimination of U(VI) ions in aqueous solution by SFeS@Biochar composites. Environmental Science and Pollution Research, 28: 55176–55185.

Liu Y., He Z., Uchimiya M. (2015): Comparison of biochar formation from various agricultural by-products using FTIR spectroscopy. Modern Applied Science, 9: 4.

Lyu P., Li L., Huang X., Xie J., Ye J., Tian Y., Huang J., Zhu C. (2023): Ternary Ca–Mg–Al layered double-hydroxides for synergistic remediation of As, Cd, and Pb from both contaminated soil and groundwater: Characteristics, effectiveness, and immobilization mechanisms. Journal of Hazardous Materials, 442: 130030.

Mohapatra L., Parida K. (2016): A review on the recent progress, challenges and perspective of layered double hydroxides as promising photocatalysts. Journal of Materials Chemistry A, 4: 10744–10766.

Musarurwa H., Tavengwa N.T. (2022): Smart metal-organic framework (MOF) composites and their applications in environmental remediation. Materials Today Communications, 33: 104823.

Obey G., Adelaide M., Ramaraj R. (2022): Biochar derived from non-customized matamba fruit shell as an adsorbent for wastewater treatment. Journal of Bioresources and Bioproducts, 7: 109–115.

Patel P.K., Pandey L.M., Uppaluri R.V.S. (2025): Conceptual techno-economic analysis of chitosan derivative resin and commercial sorbents for multi-heavy metal removal. Separation and Purification Technology, 362: 131732.

Peligro F.R., Pavlovic I., Rojas R., Barriga C. (2016): Removal of heavy metals from simulated wastewater by in situ formation of layered double hydroxides. Chemical Engineering Journal, 306: 1035–1040.

Peng H., Guo J. (2020): Removal of chromium from wastewater by membrane filtration, chemical precipitation, ion exchange, adsorption electrocoagulation, electrochemical reduction, electrodialysis, electrodeionization, photocatalysis and nanotechnology: A review. Environmental Chemistry Letters, 18: 2055–2068.

Reddy D.H.K., Lee S.-M. (2014): Magnetic biochar composite: Facile synthesis, characterization, and application for heavy metal removal. Colloids and Surfaces A: Physicochemical and Engineering Aspects, 454: 96–103.

Sanka P.M., Rwiza M.J., Mtei K.M. (2020): Removal of selected heavy metal ions from industrial wastewater using rice and corn husk biochar. Water, Air, & Soil Pollution, 231: 244.

Tan X., Liu Y., Gu Y., Xu Y., Zeng G., Hu X., Liu S., Wang X., Liu S., Li J. (2016): Biochar-based nano-composites for the decontamination of wastewater: A review. Bioresource Technology, 212: 318–333.

Tan Y., Wan X., Zhou T., Wang L., Yin X., Ma A., Wang N. (2022): Novel Zn-Fe engineered kiwi branch biochar for the removal of Pb(II) from aqueous solution. Journal of Hazardous Materials, 424: 127349.

Tang Z., Qiu Z., Lu S., Shi X. (2020): Functionalized layered double hydroxide applied to heavy metal ions absorption: A review. Nanotechnology Reviews, 9: 800–819.

Temkin M.J., Pyzhev V. (1940): Recent modifications to langmuir isotherms. Acta Physiochim, 12: 217–222.

Vithanage M., Ashiq A., Ramanayaka S., Bhatnagar A. (2020): Implications of layered double hydroxides assembled biochar composite in adsorptive removal of contaminants: Current status and future perspectives. Science of the Total Environment, 737: 139718.

Wang K., Remón J., Jiang Z., Ding W. (2024): Recent advances in the preparation and application of biochar derived from lignocellulosic biomass: A mini review. Polymers, 16: 6.

https://doi.org/10.17221/106/2025-SWR

Wang T., Li C., Wang C., Wang H. (2018): Biochar/MnAl-LDH composites for Cu (II) removal from aqueous solution. Colloids and Surfaces A: Physicochemical and Engineering Aspects, 538: 443–450.

Weber W.J., Morris J.C. (1963): Kinetics of adsorption on carbon from solution. Journal of the Sanitary Engineering Division, 89: 31–59.

Wei M., Marrakchi F., Yuan C., Cheng X., Jiang D., Zafar F.F., Fu Y., Wang S. (2022): Adsorption modeling, thermodynamics, and DFT simulation of tetracycline onto mesoporous and high-surface-area NaOH-activated macroalgae carbon. Journal of Hazardous Materials, 425: 127887.

Xu S., Zhang L., Zhao J., Cheng J., Yu Q., Zhang S., Zhao J., Qiu X. (2020): Remediation of chromium-contaminated soil using delaminated layered double hydroxides with different divalent metals. Chemosphere, 254: 126879.

Yang T., Meng J., Jeyakumar P., Cao T., Liu Z., He T., Cao X., Chen W., Wang H. (2021): Effect of pyrolysis temperature on the bioavailability of heavy metals in rice straw-derived biochar. Environmental Science and Pollution Research, 28: 2198–2208.

Zaitun Z., Halim A., Sa'dah Y., Cahyadi R. (2022): Surface morphology properties of biochar feedstock for soil amendment. IOP Conference Series: Earth and Environmental Science, 951: 012034.

Zhang X., Wang T., Xu Z., Zhang L., Dai Y., Tang X., Tao R., Li R., Yang Y., Tai Y. (2020): Effect of heavy metals in mixed domestic-industrial wastewater on performance of recirculating standing hybrid constructed wetlands (RSHCWs) and their removal. Chemical Engineering Journal, 379: 122363.

Zou Y., Liu Y., Wang X., Sheng G., Wang S., Ai Y., Ji Y., Liu Y., Hayat T., Wang X. (2017): Glycerol-modified binary layered double hydroxide nanocomposites for uranium immobilization via extended x-ray absorption fine structure technique and density functional theory calculation. ACS Sustainable Chemistry & Engineering, 5: 3583–3595.

Received: August 28, 2025
Accepted: January 6, 2026
Published online: January 20, 2026